Cell. Mol. Life Sci. (2012) 69:2765–2778
DOI 10.1007/s00018-012-0949-x

Cellular and Molecular Life Sciences

RESEARCH ARTICLE

Claudin-17 forms tight junction channels with distinct anion selectivity

Susanne M. Krug · Dorothee Günzel · Marcel P. Conrad · Rita Rosenthal · Anja Fromm · Salah Amasheh · Jörg D. Schulzke · Michael Fromm

Received: 7 December 2011 / Revised: 31 January 2012 / Accepted: 20 February 2012 / Published online: 9 March 2012

Abstract Barrier properties of tight junctions are determined by the claudin protein family. Many claudins seal this barrier, but others form paracellular channels. Among these, no claudins with general and clear-cut anion selectivity have yet been described, while for claudin-10a and claudin-4, only circumstantial or small anion selectivities have been shown. A claudin with unknown function and tissue distribution is claudin-17. We characterized claudin-17 by overexpression and knock-down in two renal cell lines. Overexpression in MDCK C7 cell layers caused a threefold increase in paracellular anion permeability and switched these cells from cation- to anion-selective. Knockdown in LLC-PK_1 cells indorsed the finding of claudin-17-based anion channels. Mutagenesis revealed that claudin-17 anion selectivity critically depends on a positive charge at position 65. Claudin-17 expression was found in two organs: marginal in brain but abundant in kidney, where expression was intense in proximal tubules and gradually decreased towards distal segments. As claudin-17 is predominantly expressed in proximal nephrons, which exhibit substantial, though molecularly not defined, paracellular chloride reabsorption, we suggest that claudin-17 has a unique physiological function in this process. In conclusion, claudin-17 forms channels within tight junctions with distinct anion preference.

Keywords Epithelium · Tight junctions · Claudin-17 · Permeability · Nephron

Abbreviations

Cldn	Claudin
DCT	Distal convoluted tubule
Occl	Occludin
PCT	Proximal convoluted tubule
tAL	Thin ascending limb of Henle
TAL	Thick ascending limb of Henle
TJ	Tight junction

Introduction

Tight junctions (TJ) are the main regulators of paracellular permeability and are localized in membranes of adjacent cells of epi- and endothelial layers. They are organized in strands consisting of transmembrane proteins and numerous associated proteins. Within the transmembrane protein components of the TJ, two types of tetraspan proteins have so far been identified: first, the TJ-associated MARVEL protein family (TAMP) [1] which consists of three members, occludin and the recently discovered proteins tricellulin [2] and MarvelD3 [3], and second, the claudin (cldn) family. In mammals, 27 different claudins have been reported, some of which also have splice variants [4].

Electronic supplementary material The online version of this article (doi:10.1007/s00018-012-0949-x) contains supplementary material, which is available to authorized users.

S. M. Krug · D. Günzel · M. P. Conrad · R. Rosenthal · A. Fromm · S. Amasheh · M. Fromm (✉)
Institute of Clinical Physiology, Campus Benjamin Franklin, Charité, Freie Universität and Humboldt Universität, Hindenburgdamm 30, 12203 Berlin, Germany
e-mail: michael.fromm@charite.de

A. Fromm · J. D. Schulzke
Division of Nutritional Medicine, Department of Gastroenterology, Campus Benjamin Franklin, Charité, Freie Universität and Humboldt Universität, Hindenburgdamm 30, 12203 Berlin, Germany

Many claudins have already been functionally characterized. Some claudins exhibit barrier properties, e.g., cldn1 [5], cldn3 [6], or cldn5 [7], while others form paracellular channels. Among these, cldn2 [8, 9], cldn15 [10], and cldn10b [11] have been shown to form cation-selective channels. So far, no claudins with general and clear-cut anion channel properties have been described. Cldn10a shows a charge selectivity for small anions, the extent of which, however, depends on the expression system used [11, 12]. Cldn4, which was originally reported to be a barrier-forming protein, has been shown to increase anion permeability when interacting with claudin-8 in M1 kidney cells [13]. The relevance of that result is unclear, as in other cell lines and tissues which express both claudins, no anion selectivity was observed [14, 15].

Little is so far known about cldn17. The gene coding for this protein is clustered with the cldn8 gene on chromosome 21q22.11. Additionally, both claudins share high sequence similarity [16]. Although they are in close proximity on chromosome 21, which suggests similar regulation under control of one promoter, expression of cldn17 has only been ascertained in the kidney by analysis of SAGE databases [17].

In the present study, cldn17 expression was found in renal tubule epithelia with gradual decrease from the proximal tubule (PCT) downstream to the distal convoluted tubule (DCT). It was also expressed in leaky renal epithelial cell lines, suggesting cldn17 has pore-forming properties. Therefore, for functional characterization, human cldn17 was expressed in MDCK C7 cells, a high-resistance subtype of MDCK cells which endogenously lacks any cldn17 expression. In an opposite approach, cldn17 was knocked down in LLC-PK_1 cells, a renal cell line that strongly expresses cldn17.

The results presented here revealed cldn17 to be a channel-forming TJ protein with definite selectivity for anions. The specific expression and functional properties of cldn17 indicate a unique physiological function in the PCT, where it allows for quantitative reabsorption of filtered anions. Thus, cldn17 is suggested to be a structural correlate of the high Cl^- permeability of the proximal nephron.

Materials and methods

Cell culture and transfections

MDCK C7 cells [18] were maintained in Dulbecco's modified Eagle medium (DMEM; Sigma-Aldrich) supplemented with 10% (v/v) fetal bovine serum (FBS; Biochrom, Berlin, Germany), 100 U/ml penicillin, and 100 μg/ml streptomycin (Sigma-Aldrich).

MDCK C7 cells were stably transfected with p3xFLAG-pCMV10 containing the human cldn17 cDNA by employing the Lipofectamine plus method (Gibco BRL). G418-resistant cell clones were screened for cldn17 expression by western blot and localization within the TJ was analyzed using immunofluorescence microscopy. MDCK C7 cells transfected with the empty vectors served as control.

LLC-PK_1 cells (ATCC) were maintained in minimum essential medium (MEM) alpha with GlutaMAX™ (no nucleosides, Invitrogen) and supplemented with 10% (v/v) fetal bovine serum (FBS), 100 U/ml penicillin, and 100 μg/ml streptomycin. Endogenous cldn17 was knocked down by transient transfection of LLC-PK_1 with pools of siRNA corresponding to gene silencer sequences to porcine cldn17 (customized at Applied Biosystems; target sequences pool 1: 5′-AACATTATTGTCTTTGAAAGG-3′, 5′-AAGTTCTACAGTTCTATGCTG-3′, 5′-AATATC-ATCATCAGGGACTTC-3′; pool 2: 5′-AAGAAGATTCAGTGCACAGGT-3′, 5′-AAGATT-CAGTGCACAGGTTCT-3′, 5′-AAGTGTTGCTGTCCTCTTCAT-3′) using Fugene HD (Promega) as suggested by the manufacturer. An unspecific scramble siRNA was used as additional control. Successful knockdown was verified by qRT-PCR and western blot after performance of dilution potential measurements.

PCR cloning of human wild-type cldn17 and generation of K65-mutants

Human kidney cDNA was used to amplify cldn17 using 5′-CCTTGGCATGGTGGGGACTC-3′ as sense and 5′-TGTGGATGGCTGGGTTGTAGAAAT-3′ as antisense primers according to the human cldn17 sequence. The resulting 675-bp product was cloned into pCR2.1-TOPO (Invitrogen), verified by sequencing and subcloned into p3x-FLAG-CMV10 (Sigma-Aldrich). Mutations of amino acid position 65 were achieved, additionally employing 5′-AGGGTCCGGTTGCAATGCGA-GTTCTATAGC-3′ as sense and 5′-CTATAGAACTCGCATTGCAACCGGACCCTG-3′ as antisense primers for K65E, and 5′-AGGGTCCGGTTGCAATGCGCGTTCTATAGC-3′ as sense and 5′-CTATAGAACGCGCATTGCAACCGGACCCTG-3′ as antisense primers for K65A.

Isolation of RNA, reverse transcription, PCR, and qRT-PCR

Murine tissue RNA as well as rotein and RNA of siRNA-treated LLC-PK_1 cells were isolated using the Nucleospin RNA/protein kit (Marcherey-Nagel, Düren, Germany) according to the manufacturer's instructions and RNA was quantified by NanoDrop® ND-1000 UV–Vis Spectrophotometer (PEQLAB Biotechnologie, Erlangen, Germany).

Next, 2 µg of total RNA per reaction were reverse-transcribed using High Capacity cDNA Reverse Transcription Kit (Applied Biosystems, Mannheim, Germany) as described by the manufacturer. Additionally, RT-minus-controls were generated for each tissue sample.

Amplification of murine cldn17 was performed using 5′-ATGGCTTTTTATCCCTTACAGATCG-3′ as sense and 5′-TTAGACGTAGCTGGTGGAAGATT-3′ as antisense primers. As control, GAPDH was amplified using 5′-GACAACTCCCTCAAGATTGTCAG-3′ as sense and 5′-CTTCTTGATGTCATCATACTTGGC-3′ as antisense primers.

Quantitative RT-PCR for porcine cldn17 of LLC-PK_1 cells was performed on a 7500 FAST Real-time PCR System using a SYBR green Assay (Applied Biosystems) according to manufacturer's instructions. Primers 5′-TATGGACAGTAACAGTGGAGAAACACATCA-3′ (sense) and 5′-CCTTTCAAAGACAATAATGTTGCTGCCA-3′ (antisense) were used. Porcine GAPDH primers 5′-GGGGAGCCAAAAGGGTCATCATCT-3′ (sense) and 5′-GACGCCTGCTTCACCACCT-TCTTG-3′ (antisense) were used as control. Differential expression was calculated according to the $2^{-\Delta\Delta CT}$ method.

Western blotting

Cells were washed with ice-cold PBS, scraped from the permeable supports, and then homogenized in lysis buffer (20 mM TRIS, 5 mM $MgCl_2$, 1 mM EDTA, 0.3 mM EGTA) containing protease inhibitors (Complete; Boehringer, Mannheim, Germany), while mice tissues were directly homogenized in lysis buffer. Membrane fractions were obtained by passing through a 26-G 1/2 needle, followed by a centrifugation at $200\times g$ for 5 min and a subsequent centrifugation of the remaining supernatant at $43{,}000\times g$ for 30 min. The resulting pellets contained the membrane proteins and were resuspended in lysis buffer. Proteins of tissues were obtained as whole protein lysates (10 mM Tris–Cl pH 7.5; 150 mM NaCl, 0.5% Triton X-100, 0.1% SDS, protease inhibitors (Complete; Boehringer).

Protein of siRNA-treated LLC-PK_1 cells was prepared in parallel to RNA samples using the Nucleospin RNA/protein kit (Marcherey-Nagel) according to the manufacturer's instructions.

Concentration of protein content was determined using BCA Protein assay reagent (Pierce) quantified with a plate reader (Tecan). Protein samples of same concentrations were mixed with SDS-sample buffer (Laemmli), denatured at 95°C for 5 min, fractionated on SDS polyacrylamide gels, and then transferred to a PVDF membrane (Perkin Elmer). Proteins were detected by immunoblotting employing primary antibodies against occludin and cldn1, -2, -3, -4, and -7 (Invitrogen), tricellulin (Pineda-Antikörper-Service, Berlin, Germany; [19]), cldn17 (Sigma-Aldrich), FLAG-M2 (Sigma-Aldrich), and β-actin (Sigma-Aldrich). After washing steps in PBST, membranes were incubated with secondary anti-mouse or anti-rabbit antibodies. For chemiluminescence detection, membranes were washed and incubated with Lumilight (Roche). Specific signals were quantified by luminescence imaging (Fusion FX7; Vilber) and quantification software (Multi Gauge V3.2; Fujifilm).

Immunofluorescence microscopy

Paraffin sections of formaldehyde-fixed murine kidneys and human kidney resections (the investigation was approved by the local ethics committee) were deparaffinized and rehydrated. This was followed by an antigen retrieval step by boiling in 10 mM sodium citrate buffer (pH 6.0) for 20 min and permeabilization with PBS containing 0.5% (v/v) Triton X-100. Blocking was performed 30 min in 5% goat- or rabbit-serum, depending on the antibodies used, in PBS containing magnesium and calcium and 30 min in immunofluorescence buffer (0.1% Triton-X 100, 0.15 M NaCl, 5 mM EDTA, 20 mM HEPES, pH 7.5). Antibodies were diluted in immunofluorescence buffer; mouse anti-cldn17 (R&D) 1:25; rabbit anti-NKCC2 (generous gift of Dr. Juliane Reiche, MDC Berlin) 1:100; rabbit anti-cldn1, -2, and -14 (Invitrogen) 1:100; goat anti-AQP-1 (Santa Cruz, Heidelberg, Germany) 1:100; Alexa Fluor 488 goat anti-mouse, Alexa Fluor 594 goat anti-rabbit, and Alexa Fluor 594 rabbit anti goat (Molecular Probes MoBiTec) 1:500.

Cells were grown on porous polycarbonate microwell inserts to confluence (Millicell-HA, area 0.6 cm^2; Millipore) to confluence, rinsed with PBS, fixed with methanol, and permeabilized with PBS containing 0.5% (v/v) Triton X-100. After blocking, antibodies were diluted in blocking solution; mouse anti-FLAG-M2 (Sigma-Aldrich) 1:600; rabbit anti-occludin (Invitrogen) 1:200; Alexa Fluor 488 goat anti-mouse and Alexa Fluor 594 goat anti-rabbit (Molecular Probes MoBiTec) 1:500.

Immunofluorescence images were obtained with a confocal laser scanning microscope (LSM 510 Meta; Zeiss), using excitation wavelengths of 543 and 488 nm.

Dilution and biionic potential measurements

Cells were grown on porous polycarbonate microwell inserts to confluence (Millicell-HA, area 0.6 cm^2; Millipore). Voltage and transepithelial resistance (R^t, Ω cm^2) were measured in Ussing chambers designed for cell filters [20]. Resistance of bathing solution and filter was measured prior to each experiment and subtracted. Ussing chambers and water-jacketed gas lifts were filled with

10 ml standard Ringer's solution [in mM: Na^+ 140; Cl^- 149.8; K^+ 5.4; Ca^{2+} 1.2; Mg^{2+} 1; HEPES 10; D(+)-glucose 10]. pH was adjusted to 7.4 with NaOH. The solution was equilibrated with 100% O_2 at 37°C.

Single ion permeabilities were determined from dilution or biionic potentials and the Goldman–Hodgkin–Katz equation as reported previously (9–12, 20). Briefly, NaCl dilution potentials were measured by switching one hemichamber to a solution containing a reduced concentration of NaCl and all other components identical to standard Ringer's (for composition, see Table S1). Osmolality was balanced by mannitol. For biionic potentials, the solution in one hemichamber was changed to one in which a part of the NaCl was replaced isoosmotically by the respective cation-chloride or sodium-anion salt.

For determination of bicarbonate permeability, O_2-equilibrated solutions 4 and 8 were used and eventual changes of pH were determined for the duration and conditions of the experiment. The observed changes were negligible ($\Delta pH = +0.22$). In a range of pH 7.4–9.4, the dissociation equilibrium is min. 90% HCO_3^-, max. 10% CO_3^{2-}, and ~1% CO_2. These distributions were considered for calculation.

Two-path impedance spectroscopy

Two-path impedance spectroscopy was performed as recently described [21]. In brief, an electric circuit model was used to describe the epithelial properties. The epithelial resistance (R^{epi}) consists of two parallel resistors, transcellular resistance (R^{trans}), which is further divided into resistors and capacitors, and the paracellular resistance (R^{para}; TJ). R^{epi} is in series to the subepithelial resistance (R^{sub}) which is caused by the filter support. After application of alternating current (35 μA/cm^2, frequency range 1.3 Hz to 65 kHz), voltage changes were detected by phase-sensitive amplifiers (402 frequency response analyzer; Beran Instruments, Glen Allen, VA, USA; and 1286 electrochemical interface; Solartron Schlumberger, Atlanta, GA, USA). Complex impedance (Z_{real}, $Z_{imaginary}$) values were calculated and plotted in a Nyquist diagram. R^{trans} and R^{para} were determined from experiments in which the impedance spectra and fluxes of a paracellular marker substance, fluorescein, were obtained before and after chelating extracellular Ca^{2+} with EGTA. This caused TJs to open and to increase fluorescein flux. It was ascertained in separate experiments that changes of fluorescein fluxes are inversely proportional to R^{epi} changes.

Flux measurements of fluorescein and ^{36}Cl

All flux studies were performed in Ussing chambers under short-circuit conditions. For fluorescein fluxes, Ussing chambers were filled with 10 ml Ringer's per side, 10 μl of fluorescein (100 mM) were added apically, and basolateral samples (300 μl) were replaced with fresh Ringer's 0, 10, 20, 30, and 40 min after addition. Samples were analyzed with a fluorometer (Spectramax Gemini; Molecular devices) at 520 nm (fluorescein).

Fluxes of ^{36}Cl were measured in 10 ml of Ringer's. Apically, 30 kBq of ^{36}Cl-labeled NaCl (10 mM; Biotrend) were added and a 100-μl sample was taken from the donor side, and 900 μl Ringer's and 4 ml of Ultima Gold high flashpoint liquid scintillation cocktail (Packard Bioscience) were added. Basolateral samples of 1 ml were taken 0, 30, 60, 90, and 120 min after addition and replaced with fresh Ringer's. Samples were mixed with 4 ml of liquid scintillation cocktail and were subsequently analyzed with a Tri-Carb 2100TR Liquid Scintillation counter (Packard).

Fluxes were calculated as increase in tracer quantity (corrected for dilution) per time unit and filter area (0.6 cm^2). Permeabilities were calculated as flux/concentration on the donor side.

Measurements of water permeability

Water permeability was measured as recently described by Rosenthal et al. [22]. In brief, cells were seeded on cell culture inserts and grown to confluence. Filters were mounted into modified Ussing chambers with glass tubes instead of gas lifts and maintained in HEPES buffered Ringer's solution. Generation of a transepithelial osmotic gradient with mannitol (100 mM) induced water passage, and the fluid level in both chamber tubes was monitored by a video optic system ColorView XS (Olympus Soft Imaging Solutions), at time 0 min and every 15 min over a period of 2 h. Water flux was calculated from the difference between the menisci at the recording times. Water permeability was calculated from $P = J/\Delta c$ with P = permeability (cm/s), J = flux (mol h^{-1} cm^{-2}), and c = concentration (mol/l).

Freeze-fracture electron microscopy

Freeze-fracture electron microscopy was performed as previously described [23]. Briefly, cells grown on permeable supports were fixed with phosphate-buffered glutaraldehyde (2%). Preparations were incubated in 10% (v/v) and then in 30% (v/v) glycerol and finally frozen in liquid nitrogen-cooled Freon 22. Cells were fractured at −100°C and shadowed with platinum and carbon in a vacuum evaporator (Denton DV-502). Replicas were bleached with sodium hypochloride, picked up on grids (Ted Pella), and analyzed with a video-equipped Zeiss 902A electron microscope (Olympus iTEM Veleta; Carl Zeiss).

Morphometrical analysis was performed at a final magnification of 51,000×. Vertical grid lines were drawn at 200-nm intervals perpendicular to the most apical TJ strand [24]. The number of strands horizontally oriented within the main TJ meshwork were counted at intersections with grid lines. The distance between the most apical and contra-apical strand was measured as the meshwork depth. Strand discontinuities within the main compact TJ meshwork of >20 nm were defined as "breaks" and given per micrometer length of horizontally oriented strands. Strand formation was noted as "particle type" or "continuous type". The pattern of strand loops was denoted as "angular type" or "curved type".

Statistical analysis

Data are expressed as mean values ± standard error of the mean (SEM) indicating n as the number of single measurements. Statistical analysis was performed using Student's t test with Bonferroni-Holm correction for multiple testing. $p < 0.05$ was considered significant ($^{*}p < 0.05$, $^{**}p < 0.01$, $^{***}p < 0.001$).

Results

Claudin-17 is predominantly expressed within proximal segments of the nephron

Cldn17 protein expression was investigated in brain, lung, skin, kidney, and various segments of the gastrointestinal tract, and was detectable in only two of these tissues, abundantly in the kidney and slightly in brain tissue (Fig. 1a). Bands of higher size appearing in several tissues turned out to be unspecific, as RT-PCR results confirmed the finding of cldn17 being present only in kidney and brain (Fig. 1b). Of several epithelial cell lines of epidermal, renal, and intestinal origin tested, cldn17 was strongly detectable only in kidney cell lines which exhibited low transepithelial resistances (R^{t}) typical for leaky, mainly proximal regions of the nephron (Fig. 1c). Therefore, cldn17 was hypothesized to be typically expressed in the PCT.

Further analysis of its renal expression pattern within murine (Fig. 2) and human nephron segments (Fig. S1) demonstrated cldn17 to occur mainly in the PCT (Fig. 2a), but less pronounced in subsequent segments down to the DCT. Cldn17 was present in the thin ascending limb of Henle's loop (tAL; segment marker ClC-K; Fig. 2b) as well as in the thick ascending limb of Henle's loop (TAL; segment marker NKCC-2; Fig. 2c). In the DCT (segment marker NCCT; Fig. 2d), cldn17 expression seemed to be less regular, as only a few

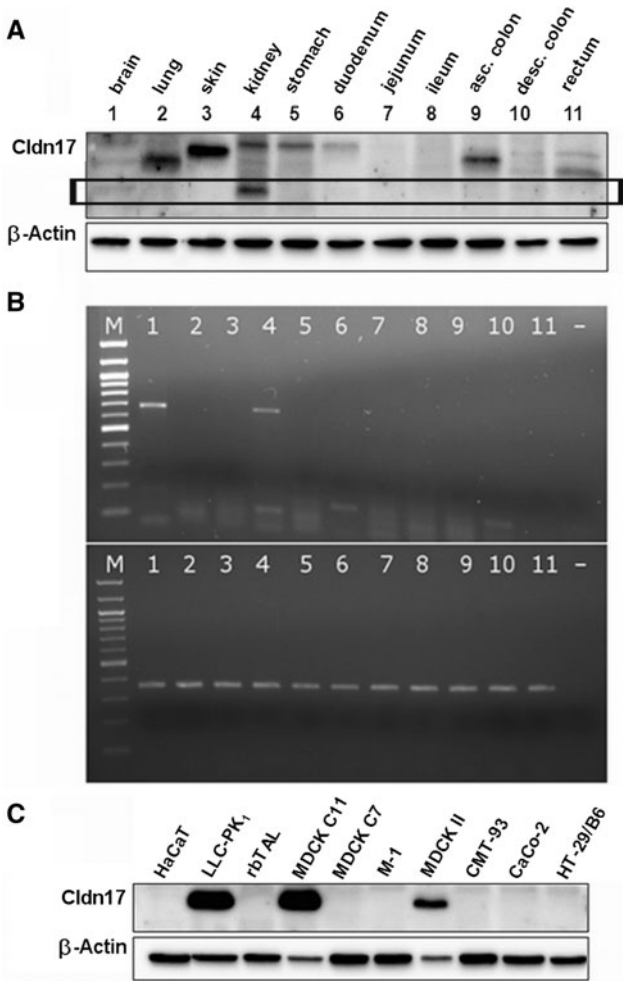

Fig. 1 Endogenous expression of cldn17. **a** Whole protein lysates of different mouse tissues. The *horizontal box* indicates the expected size of murine cldn17 (~25 kDa). **b** mRNA expression of cldn17 (674 bp) within different mouse tissues. *M* 100-bp marker (NEB), *1–11* correspond to those of (**a**), while the *rightmost* represents the no RT-control. **c** Membrane protein fractions of different epithelial cell lines as indicated. HaCaT cell were cultured in high Ca^{2+} conditions. Expression of cldn17 was found in low-resistance cell lines of renal origin

NCCT-positive tubules showed coexpression of cldn17. In the collecting duct (segment marker AQP-2; Fig. 2e), no cldn17 expression was found. In general, colocalization with occludin confirmed localization of cldn17 within the TJ (Fig. 2f).

Cldn17 was also expressed in brain tissue but much less pronounced than in the kidney. Immunofluorescent stainings of murine brain–coronal sections revealed cldn17 to be localized within membranes of vessels, which were also positive for occludin and for caveolin-1, a marker of endothelial tissue (Fig. S2). Because this study was focused on kidney tissue, where cldn17 is predominantly expressed, potential functions of cldn17 within the brain tissue and blood–brain barrier were not analyzed.

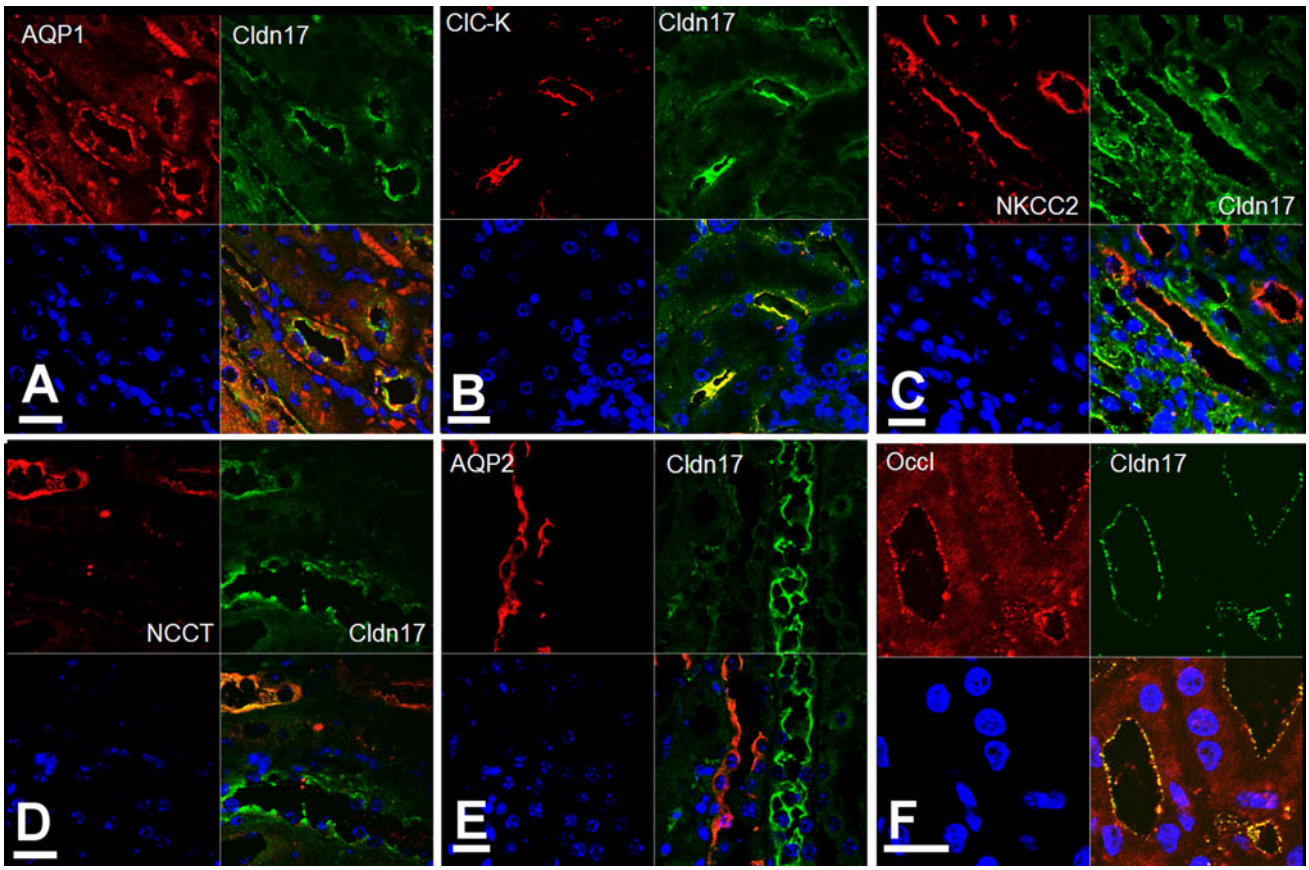

Fig. 2 Endogenous localization of cldn17 within the murine nephron. Immunofluorescent stainings. *Bars* 20 µm. **a** AQP-1 and cldn17 were colocalized within the PCT and the tAL. **b** ClC-K and cldn17 were colocalized within the tAL. **c** NKCC2 and cldn17 were colocalized within the TAL. **d** NCCT and cldn17 were occasionally colocalized within the distal tubule, as there were also areas only positive for NCCT. **e** AQP-2, a marker of the collecting duct, and cldn17 were not found in colocalization. **f** Staining of occludin and cldn17 confirmed colocalization within the TJ

Exogenous expression of claudin-17 decreases the paracellular resistance

For characterization of cldn17, MDCK C7 cells which lack expression of cldn17 (Fig. 1c) were stably transfected with N-terminal 3× FLAG-tagged human cldn17. In comparison to vector-transfected controls, strong expression of cldn17 was detectable in membrane protein fractions, and three clones were chosen for detailed analysis (Figs. 3, 4).

Overexpression of cldn17 did not alter the expression levels of other TJ proteins, occludin, tricellulin, cldn1, cldn4 or cldn7 (Fig. 3). Cldn2 was not expressed in MDCK C7 cells (9, 7). For cldn3, which has been shown to be a barrier-forming TJ protein (6), an increase was observed in clone CLDN17#10 ($114.8 \pm 2.0\%$ of controls; $^{***}p < 0.001$, $n = 4$). However, such an increase in cldn3 should not contribute to increased but to decreased permeabilities, therefore this clone was included in the present study. Correct localization of cldn17 within the TJ in colocalization with occludin as TJ marker was verified in immunofluorescent stainings (Fig. 4).

Paracellular resistance (R^{para}) reflecting the resistance of the TJ, and transcellular resistance (R^{trans}) reflecting the apical and basolateral cell membranes were determined by two-path impedance spectroscopy. The epithelial resistance (R^{epi}) represents the contribution of both R^{para} and R^{trans} in parallel. In controls, R^{para} was higher than R^{trans}, which is typical for tight epithelia. This resulted in R^{epi} of $1{,}831 \pm 179\ \Omega\ cm^2$ (Fig. 5). In contrast, R^{para} was decreased in clones transfected with cldn17, and resulted in decreased R^{epi}. For CLDN17#10 and CLDN17#19, R^{trans} was unaltered, but in CLDN17#7, R^{trans} was reduced. Because changes in transcellular parameters could interfere with paracellular effects and thus falsify our results, this clone was excluded from further discussion of the experiments.

Thus, cldn17 expression in MDCK C7 cells turned this primordially "tight" epithelium ($R^{trans} < R^{para}$) into a "leaky" one ($R^{trans} > R^{para}$). The strong decrease in R^{para} to

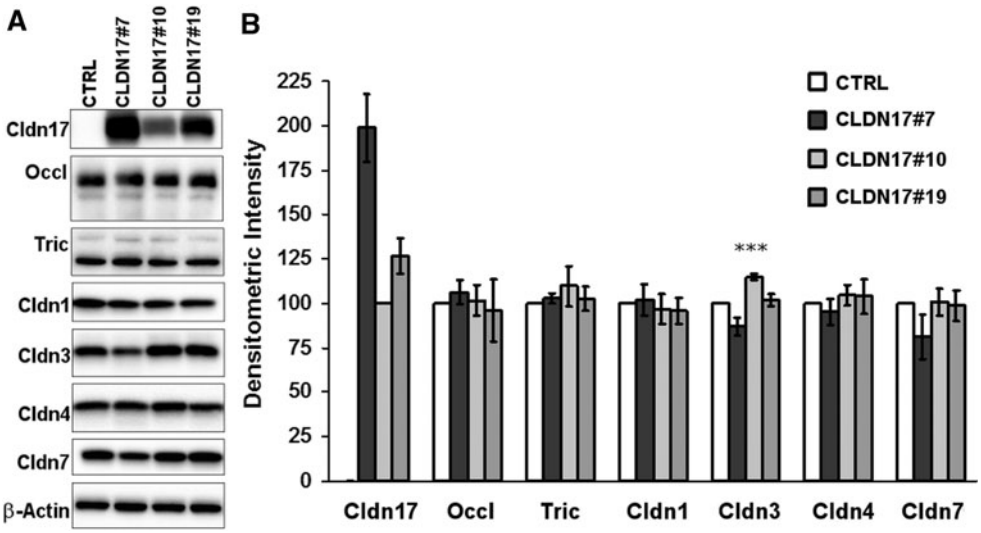

Fig. 3 Expression and localization of 3× FLAG-cldn17 and expression of other TJ proteins. **a** Cldn17, occludin, tricellulin, cldn1, cldn3, cldn4, and cldn7 were detected by western blotting in vector-transfected controls and three cldn17-overexpressing clones. β-Actin was blotted as loading control. **b** Cldn17 is strongly expressed in 3× FLAG-cldn17-transfected cells, while vector controls exhibit no cldn17 expression. Therefore, cldn17 expression was compared only between clones and clone CLDN17#10 was set 100% ($n = 4$)

approximately 20% of control values proves cldn17 to be a channel-forming TJ protein.

Claudin-17 forms paracellular channels for chloride and bicarbonate

In order to detect a possible charge preference of the cldn17 channel, permeabilities for Na^+ and Cl^- were determined measuring NaCl dilution potentials (bath solutions, see Table S1, used here: 4/4 → 4/7). As the main result, in controls, negative dilution potentials indicated slight cationic charge preference, while in cldn17-expressing clones, a change to positive potential values indicated preference for anions (Fig. 6a).

The potential influence of HCO_3^- was analyzed by repetition of dilution potential measurements in presence of 21 mM HCO_3^- equilibrated with 5% CO_2/95% O_2 (solution 1/1 → 1/2). The resulting potentials were unchanged for controls, but significantly attenuated in cldn17-expressing clones (Fig. 6a). This indicated that the permeability for HCO_3^- was also increased by cldn17 so that HCO_3^- short-circuited the potentials evoked by the Cl^- gradient. Therefore, permeabilities for Na^+ and Cl^- and the resulting ratios were calculated using HCO_3^--free conditions. The ratio P_{Na}/P_{Cl} in controls showed slight charge-preference for cations, while this ratio changed to anion preference in cldn17-expressing cells (Fig. 6b). The resulting permeabilities for Cl^- without influence of HCO_3^- were threefold elevated in comparison to controls (Fig. 6c, white bars).

An independent line of evidence was obtained by direct measurements of ^{36}Cl fluxes (Fig. 6c, gray bars). The fluxes were measured in absorptive direction and represent paracellular Cl^- permeation because MDCK C7 cells do not feature absorptive membrane transport systems for Cl^-. The increase in permeability for anions after overexpression of cldn17 was fully confirmed. Although absolute permeabilities obtained from dilution potentials and from ^{36}Cl fluxes were slightly different, the obtained increases in Cl^- permeability were in excellent agreement for both methods, namely by a factor of ~ 3.

Transient knockdown of claudin-17 confirms the overexpression experiments

In order to corroborate the results obtained by cldn17 overexpression in cells with no endogenous expression of that cldn, transient knockdown (KD) of cldn17 was performed in LLC-PK_1 cells, which possess high endogenous expression of cldn17. Three days after transfection, the cldn17 mRNA level was reduced, while unspecific scramble siRNA produced no effect (Fig. 7a). Protein levels were reduced 4 days after KD (Fig. 7b, c).

Although the KD was not strong enough to induce significant changes in R^t, dilution potential measurements revealed a decrease in the ratio P_{Cl}/P_{Na} (Fig. 7d). Thus, a cell line with high genuine anion selectivity developed a reduced preference for anions after KD of cldn17, endorsing cldn17 as TJ protein-forming paracellular anion channels. Furthermore, as LLC-PK_1 cells endogenously express cldn2, expression of this paracellular channel for cations and water was analyzed to exclude possible artifacts. However, no change of cldn2 expression was observed (Fig. 7c).

The claudin-17 channel carries anions smaller than fluorescein

To characterize cldn17-induced changes in ion permeabilities in more detail, permeability sequences of monovalent cations and anions (Eisenman sequences) as well as divalent cations (Sherry sequences) were analyzed.

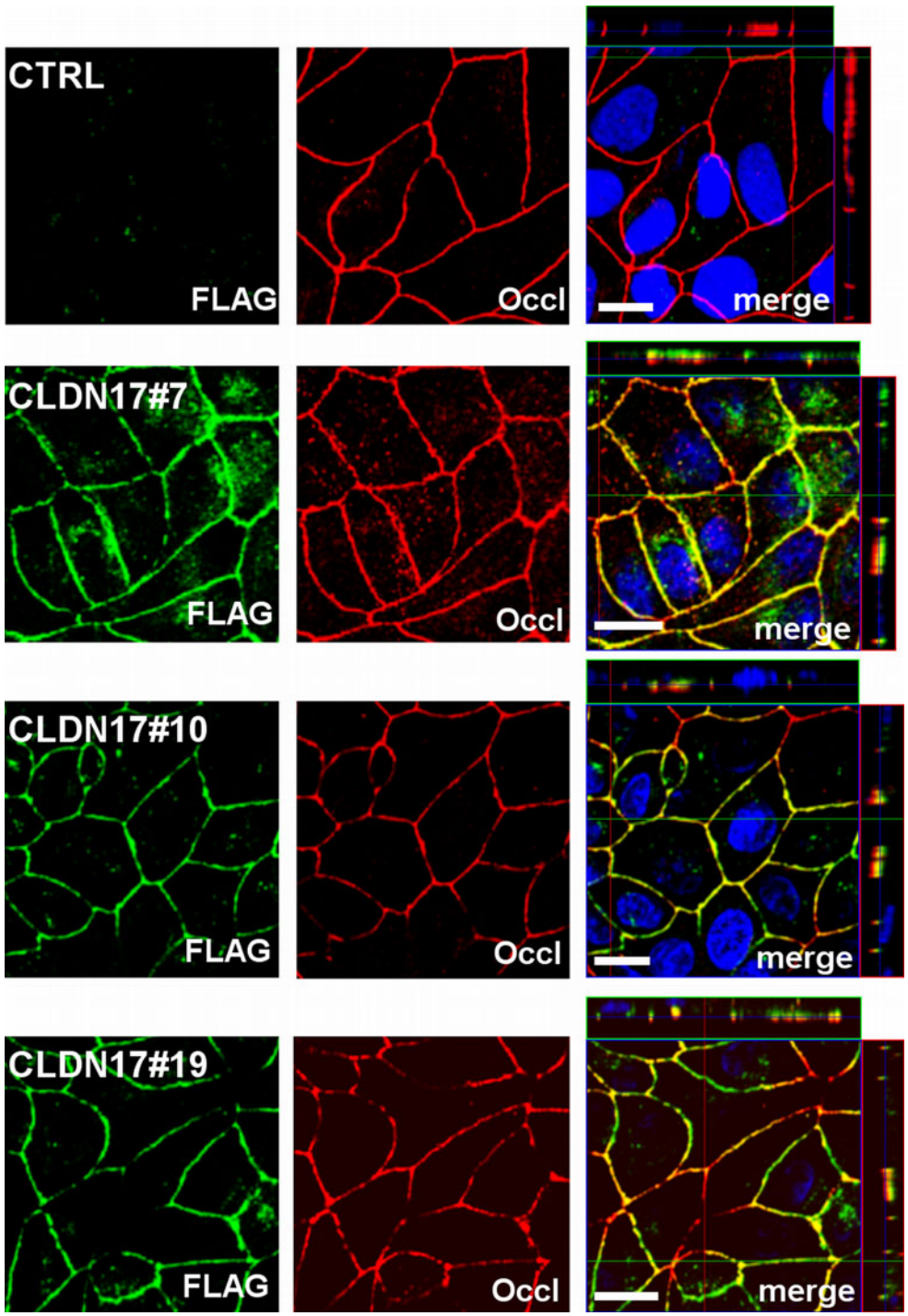

Fig. 4 Localization of 3× FLAG-cldn17 and expression of other TJ proteins. Z-scans of immunofluorescent stainings of the overexpression clones showed good colocalization of exogenous 3× FLAG-cldn17 with occludin serving as TJ marker (*bars* 20 μm)

These sequences allow for concluding on the mode of interaction between a conducting pore and permeating ions. The order of decreasing permeabilities for monovalent cations of controls yielded an Eisenman sequence IV–VII ($K^+ > Na^+ \geq Rb^+ \geq Li^+ \geq Cs^+$) and overexpression of cldn17 only marginally changed this result (Fig. 6a). For divalent cations, Sherry sequences VI–VII ($Mg^{2+} \geq Ca^{2+} > Sr^{2+} > Ba^{2+}$) were also found in controls and both clones (Fig. 8b). This indicates that cldn17 overexpression had no noticeable effect on cation permeability, which is in accordance with the predominant anion selectivity of that cldn.

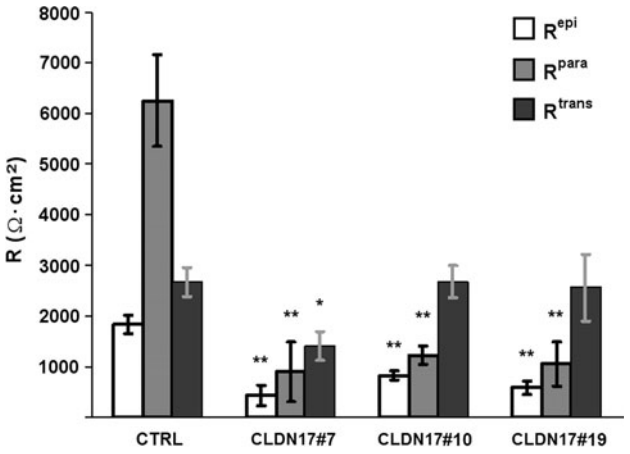

Fig. 5 Two-path impedance spectroscopy. Expression of cldn17 induced a decrease of R^{epi} which was caused by a 5- to 6-times drop of R^{para}. R^{trans} was only changed in clone cldn17#7 leading to exclusion of this clone from subsequent experiments ($*p < 0.05$, $**p < 0.01$, $n = 4$–5)

Determination of the permeabilities for monovalent anions resulted in Eisenman sequence VII ($F^- > Cl^- > Br^- > I^-$) in controls. In contrast to the above cation permeabilities, anion permeabilities in cldn17-overexpressing clones were three times elevated, and the sequence was shifted to Eisenman sequence IV ($Cl^- > Br^- > I^- > F^-$). This indicates less interaction with the hydration shell of anions in those clones than in controls (Fig. 8c). Measurement of permeabilities for other anions (Fig. 8d) revealed an increased passage of pyruvate after overexpression of cldn17.

For permeability of HCO_3^-, calculations using the difference in potentials obtained under HCO_3^--free and -containing conditions (Fig. 6a) were performed. The relative HCO_3^- permeability (P_{HCO3}/P_{Na} or P_{HCO3}/P_{Cl}) revealed a general increase of HCO_3^- permeability after cldn17-overexpression. However, as the experimental system was very sensitive to even slight potential changes, absolute values were not achieved because large fluctuations also occurred in the controls that were unaffected by HCO_3^-. Thus, biionic potentials were measured (Fig. 8d) and resulted in permeabilities comparable to those for pyruvate.

The permeability for a larger anion, the paracellular flux marker fluorescein (332 Da, Stokes radius $\sim$4.5 Å), was lower and not significantly changed. This result leads to the conclusion that the paracellular channel formed by cldn17 is not only charge- but also size-selective for solutes smaller than $\sim$9 Å in diameter.

Claudin-17 does not form water channels

Water permeability was determined by measurement of osmotically driven water flux. Comparison of vector controls with cldn17-expressing clones revealed no alteration in water permeability. Additionally, no changes in expression of AQP-1, -3, and -4, which are expressed in MDCK C7, were observed; thus, cldn17 has no significant effect on paracellular water permeability.

Claudin-17 anion selectivity critically depends on a positively charged amino acid at position 65

Within the extracellular loop 1 of channel-forming claudins, the amino acids directly following the second of the two conserved cysteins (position 65 in cldn17) are believed to be crucial for charge-selectivity (15–16). Comparison of cldn17 with cldn2 and cldn10a revealed this position to be positively charged in cldn17 (lysine) and cldn10a (arginine), which are both anion-selective (Fig. 9a). In contrast, this position was negatively charged in cldn2. Mutagenesis

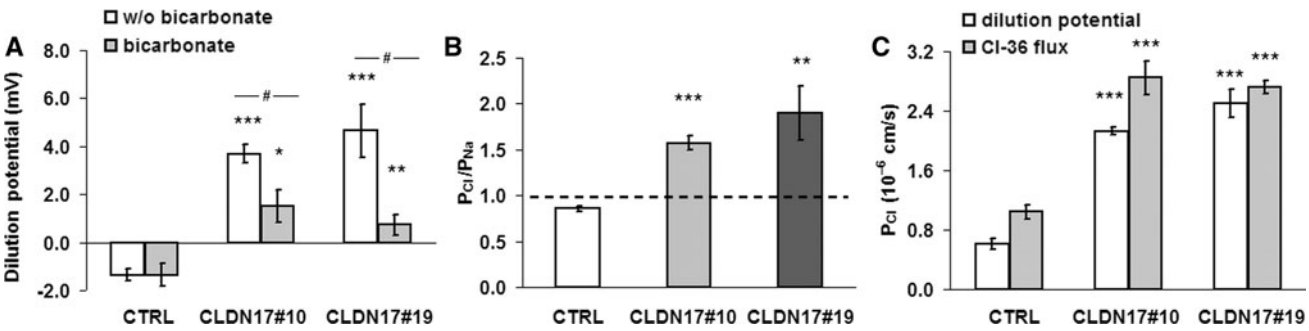

Fig. 6 Dilution potentials, P_{Cl}/P_{Na}, and P_{Cl}. **a** Changes in dilution potentials from negative to positive values were observed in cldn17-expressing cells, indicating reversal in charge-selectivity. Under HCO_3^--containing conditions, the potential changes were attenuated ($^{\#}p < 0.05$), but still reflected the change to anion selectivity. **b** The ratio P_{Cl}/P_{Na} was calculated from dilution potential measurements under HCO_3^--free conditions. The resulting ratio revealed charge-preference for anions in cldn17-expressing cells ($n = 6$). **c** Permeability for Cl^-, obtained by dilution potential measurements under HCO_3^--free conditions (*white bars*; $***p < 0.001$, $n = 6$) and by flux measurements of $^{36}Cl^-$ (*gray bars*; $***p < 0.001$, $n = 6$–8). In both setups, the Cl^- permeability was increased about threefold in cldn17 clones

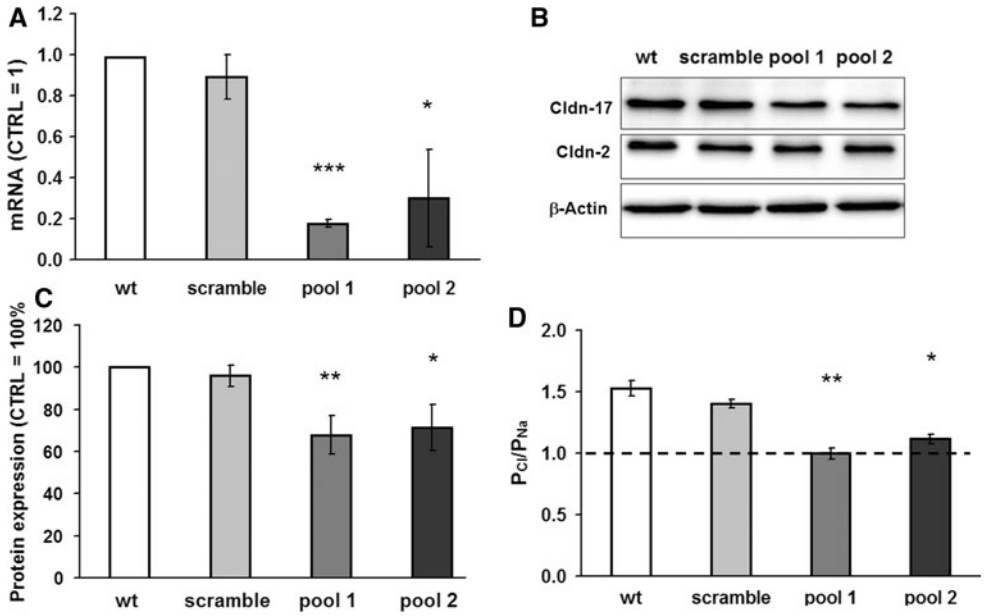

Fig. 7 Cldn17 knockdown (KD) experiments in LLC-PK_1 cells. **a** mRNA levels of cldn17 before and after KD in LLC-PK_1. After treatment with specific siRNAs, cldn17 mRNA was reduced to 20% (***$p < 0.001$) and 30% (*$p < 0.05$), while scramble siRNA had no effect on cldn17 mRNA ($n = 3$). **b** Exemplary western blots for KD of cldn17 ($n = 4$–5). Expression of cldn17 was downregulated after treatment with specific siRNAs, while the scramble control showed no expression change. Cldn2 was unaffected by siRNA treatment. β-Actin was blotted as loading control. **c** Protein fractions of cells transfected with cldn17-siRNA showed markedly reduced expression of cldn17 ($n = 4$–5). **d** The P_{Cl}/P_{Na} ratio was changed to lowered preference for anions after cldn17 KD (*$p < 0.05$, $n = 4$–6)

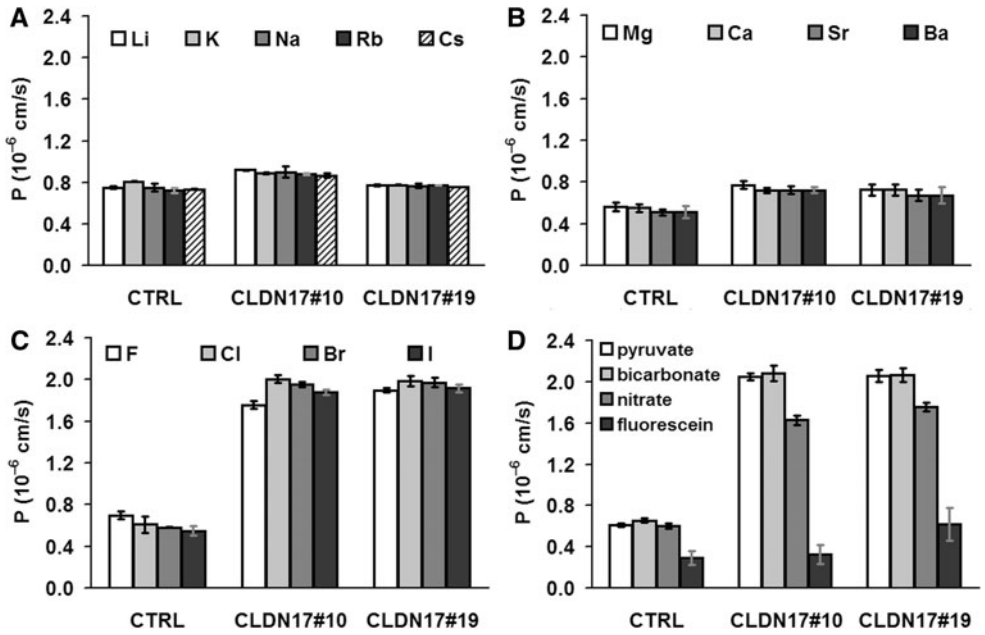

Fig. 8 Permeabilities for different ions comparing vector controls and cldn17-transfected cells. **a** Monovalent cations. Permeabilities for monovalent cations were only marginally increased ($n = 6$). **b** Divalent cations. Permeabilities for divalent cations resulted in Sherry sequences VI–VII for the vector-transfected cells and for cells transfected with cldn17. These clones showed a negligible increase of permeabilities ($n = 6$). **c** Monovalent anions. Permeabilities for monovalent anions resulted in Eisenman sequence VII for the vector-transfected cells and IV for cldn17-expressing clones. Generally, permeabilities for all measured anions were dramatically increased (***$p < 0.001$, $n = 6$). **d** Other anionic solutes. Permeabilities for the anions pyruvate, HCO_3^-, and NO_3^- were increased in cldn17-expressing clones (***$p < 0.001$, $n = 6$), whereas permeability for fluorescein was unchanged ($n = 6$)

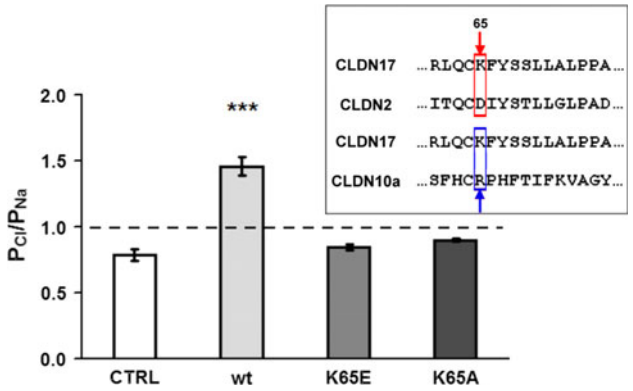

Fig. 9 Dilution potentials P_{Cl}/P_{Na} of cldn17 mutated position K65. The ratio P_{Cl}/P_{Na} under HCO_3^--free conditions revealed a charge-preference for anions in cldn17-expressing cells which was impeded in K65E as well as in K65A (***$p < 0.001$, $n = 5$–6). *Insert* sequence alignment of the region around amino acid 65 of human CLDN17, CLDN2, and CLDN10a. The anion-selective channels cldn17 and cldn10a have a positively charged amino acid in position 65, while cldn2 possesses the negative charged amino acid aspartate

from lysine to aspartate, the negatively charged amino acid present in cldn2 at that position, resulted in changes of the ratio P_{Cl}/P_{Na} (Fig. 9b). While wild-type cldn17-overexpressing cells showed a shift to anion selectivity in comparison to controls, the mutant K65D exhibited no effect on permeability ratio. Even the mutation K65A, an uncharged amino acid, resulted in permeability ratios similar to vector controls.

Tight junction ultrastructure is unchanged after claudin-17 overexpression

Freeze-fracture electron micrographs were morphometrically analyzed with respect to the number of horizontal strands, compact meshwork depth, density of strands, breaks per micrometer single strand, the ratio of particle/continuous type, and the ratio of angular/curved type. A comparison of controls and cldn17-transfected clones revealed no significant changes in any of the tested parameters (Table S1; Fig. S3).

Discussion

It has long been known that in the proximal nephron, anions are, in part, paracellularly reabsorbed, but the molecular basis for that transport pathway has not yet been disclosed. It was the aim of the present study to identify and characterize TJ proteins underlying this renal paracellular anion transport. Here, we describe cldn17 protein expression to predominate in the nephron, especially in the PCT, and to a much lesser extent in brain tissue. The clustering of cldn17 with cldn8 on chromosome 21 might indicate regulation of expression through a common promoter, and homology between both claudins might suggest a similarity in function. Even so, function as well as tissue distribution are complementary in cldn17 and cldn8. In contrast to cldn 17, cldn8 is expressed predominantly in the distal parts of the nephron [25], and has been reported to reduce both cation and anion permeability when overexpressed in MDCK II cells [26]. The mechanism for cldn8-induced tightening against cations was demonstrated to be a down-regulation of cldn2 expression [27]. Whether or not a parallel mechanism exists against anions caused by a down-regulation of cldn17 will be the subject of future investigation.

For functional characterization of cldn17, we performed both overexpression and KD studies and found it to be a paracellular channel-forming TJ protein with definite selectivity for inorganic and small organic anions. For overexpression, MDCK C7 cells were chosen, because they show no endogenous expression of cldn17. As these cells also do not express other known channel-forming TJ proteins, e.g., cldn2 [22], cldn10 [11, 12] or cldn15, any influence of those was excluded.

Analysis of electrophysiological properties of cldn17 overexpression clones revealed cldn17 to form paracellular channels preferentially selective for anions, although permeability for cations was also slightly increased. Overexpression switched the charge-selectivity of MDCK C7 cells from cationic to anionic. Cldn17 turned out to be not only charge- but also size-restrictive, because the permeability for the inorganic anions NO_3^-, HCO_3^-, and small organic anions such as pyruvate, but not for the larger organic anion fluorescein, were increased.

In order to obtain an independent line of evidence for cldn17 function as a paracellular anion channel, we used the opposite approach, i.e., cldn17-KD. For this, we employed the kidney cell line, LLC-PK_1, which also serves as a model for PCT cells, but in contrast to MDCK C7 cells, endogenously expresses cldn17. These studies fully confirmed cldn17 as a clear-cut anion-selective TJ protein.

Paracellular water permeability has been demonstrated [22] for the cation channel former cldn2 [9], a cldn abundant in PCTs [28, 29]. Thus, it appeared obvious to investigate whether or not cldn17 also conveys relevant water permeability. Comparison of MDCK C7 vector controls with cldn17-overexpressing clones revealed no significant alteration in water permeability. Thus, in contrast to cldn2, cldn17 is not a paracellular channel for water.

In freeze-fracture electron micrographs, the TJ is sometimes found to be changed by altered cldn composition so that permeabilities may be affected by such changes. This was excluded, as in a detailed morphometric analysis, no significant changes were detected after cldn17 overexpression. This is in line with observations for cldn2

and cldn10b. Expression of these TJ proteins in MDCK C7 cells did not lead to strand discontinuities [22]. On the other hand, in some cell lines and tissues, strand discontinuities were observed after expression of cldn2 [30], indicating that the TJ strand appearance seems to also depend on the endogenous TJ protein background. Thus, in MDCK C7, cldn2, cldn10b, and cldn17 did not induce strand discontinuities.

The question then arises concerning the physiological function of the cldn17 anion channel. Cldn17 turned out to be segmentally distributed along the nephron, with a main expression site in the PCT, decreasing expression in the subsequent segments, and no expression in the DCT. This pattern parallelled the general scheme of decreasing ion conductance from proximal to distal segments, which is in full accordance with our finding that cldn17 could contribute to that conductance.

The PCT is the site of highest Cl^- reabsorption. Two pathways are involved: an active transcellular and a passive paracellular one. For Cl^-, the overall fraction is assumed to be about equal for each route [31, 32] with higher values in the early PCT (S1 segment), where a lumen-negative voltage drives the transport, and lower values in the subsequent segments (S2 and S3), where a concentration gradient for Cl^- drives Cl^- reabsorption.

So far, two TJ proteins present in the nephron have been suggested to contribute to paracellular anion transport, cldn4 and cldn10a, but their effects on Cl^- permeability were circumstantial or weak, respectively. Cldn4, not present in the proximal segments, has been reported to form Cl^--selective paracellular channels in the collecting duct. This feature, however, becomes effective only in association with cldn8 [13], and it is difficult to generalize this finding, because in other tissues possessing both claudins, no increase in anion permeability has been observed [14, 15]. Cldn10a, which has been shown to be present in PCT S2 segments [29], was characterized in overexpression studies in several cell lines as a channel featuring anion selectivity [11, 12]; however, the effects were weak compared to cldn17. For example, overexpression of cldn10a in MDCK C7 cells, which were also used in the present study, decreased R^t, but did not increase Cl^-permeability, only that for NO_3^- [11]. Although HCO_3^- permeability was not explicitly investigated in Cldn10a overexpressing cells, data obtained in the presence and absence of HCO_3^- presented in Günzel [11] (compare P_{Cl}/P_{Na} values of their fig. 6b obtained in the absence of HCO_3^- with P_{Na}/P_{Cl} values in their fig. 7a obtained in the presence of HCO_3^-) indicate that cldn10a has no effect on the permeability for HCO_3^-.

In contrast, cldn17 greatly enhanced not only Cl^- and NO_3^- but also HCO_3^- permeability. This finding is intriguing, as HCO_3^- transport in the PCT is of fundamental importance for acid-base regulation of the organism. More than 80% of the filtered HCO_3^- are reabsorbed within the PCT [33], predominantly via transcellular routes, but most of the carbonic anhydrase-independent reabsorption takes place via paracellular transport [34]. The paracellular HCO_3^- reabsorption depends on proton secretion [35]. HCO_3^- is generated during acid excretion to maintain the acid–base balance. To replenish its loss during the titration of nonvolatile acids, it has to be reabsorbed by the nephron. As cldn17-expressing cells showed a strong increase of permeability for this anion, it might also play a major role for paracellular HCO_3^- transport.

In summary, cldn17 conveys a high capacity paracellular transport pathway for inorganic and, as will be discussed below, for small organic anions. It is thus highly charge-selective but does not sharply discriminate between different anion species. In contrast, cldn10a is only permeable for small inorganic anions excluding HCO_3^-.

The differences in permeability properties between cldn17 and cldn10a must be related to the pore size of cldn17. NO_3^- permeability increased and the ratio P_{NO_3}/P_{Na} increased from values <1 in controls to values >1 in cldn10a-transfected cells, indicating a reversal of charge preference for this ion. In sharp contrast to cldn17 which greatly increased pyruvate permeability, overexpression of cldn10a lowered pyruvate permeability of MDCK C7 cells. This already suggests that cldn10a may form an anion channel with a smaller pore diameter than that of cldn17. The larger pore diameter of cldn17-based channels is further indicated by the finding that the relative permeability for F^-, an anion of small unhydrated but very large hydrated diameter, increases less than permeabilities of the other halide anions (Cl^-, Br^-, I^-). This implies that cldn17-based pores are not able to fully remove the F^- hydration shell and, in terms of the Eisenman theory, presents a weak field strength binding site. Plotting the increase of permeability for the analyzed anions after cldn17 overexpression against the unhydrated ion diameters—with F^- as exception—results in a linear relationship.

This indicates a pore diameter between 9 and 10 Å (Fig. 10), which is also in line with the finding that the permeability for fluorescein is not significantly altered. Interestingly, this pore size does not convey significant water permeability, although the pore diameter of cldn2, the only paracellular water channel discovered so far [22], is slightly smaller [36]. This indicates that the electrostatic interaction site as determined by charged amino acids of the ECL1 may influence the permeation of water and not the pore size which is considered wider than needed to let a single water molecule pass through [26, 37].

Comparison of the ECL1 amino acid sequences of cldn17, cldn10a, and cldn2 revealed similarities between

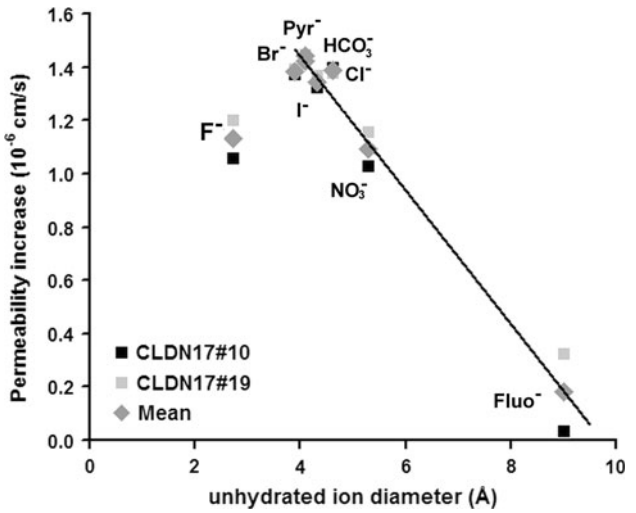

Fig. 10 Size estimation of the cldn17 channel. Permeability increases of CLDN17#10 (*black square*), CLDN17#19 (*gray square*) and their mean (*gray rhombus*) showed a linear relationship to the unhydrated ion diameters. An exception was F^-. The linear extrapolation suggests a cldn17 pore diameter of 9–10 Å

cldn10a and cldn17. The amino acid at position 65 has been identified as the most discriminative position within ECL1 for charge selectivity [36, 38]. In that position, cldn17 as well as cldn10a possess a positively charged residue (lysine, arginine), while cldn2 features the negatively charged residue aspartate (Fig. 9a).

We found that mutation of position 65 from a positively to a negatively charged amino acid resulted in a loss of anion selectivity of wild-type cldn17. Even a mutation of position 65 to a neutral amino acid caused a loss of anion selectivity. Thus, a positive amino acid at position 65 is crucial for the anion selectivity of cldn17.

In conclusion, cldn17 forms paracellular channels with unique anion selectivity. As cldn17 is predominantly localized in proximal segments of kidney tubules, we suggest that it forms the molecular basis of paracellular Cl^- and HCO_3^- transport in these segments.

Acknowledgments We would like to thank In-Fah M. Lee and Detlef Sorgenfrei for their excellent technical assistance. This work was supported by grants of the Deutsche Forschungsgemeinschaft (DFG FOR 721) and the Sonnenfeld-Stiftung Berlin.

Conflict of interest The authors declare that they have no conflicts of interest.

References

1. Raleigh DR, Marchiando AM, Zhang Y, Shen L, Sasaki H, Wang Y, Long M, Turner JR (2010) Tight junction-associated MARVEL proteins MarvelD3, tricellulin, and occludin have distinct but overlapping functions. Mol Biol Cell 7:1200–1213
2. Ikenouchi J, Furuse M, Furuse K, Sasaki H, Tsukita S, Tsukita S (2005) Tricellulin constitutes a novel barrier at tricellular contacts of epithelial cells. J Cell Biol 171:939–945
3. Steed E, Rodrigues NT, Balda MS, Matter K (2009) Identification of MarvelD3 as a tight junction-associated transmembrane protein of the occludin family. BMC Cell Biol 10:95
4. Mineta K, Yamamoto Y, Yamazaki Y, Tanaka H, Tada Y, Saito K, Tamura A, Igarashi M, Endo T, Takeuchi K, Tsukita S (2011) Predicted expansion of the claudin multigene family. FEBS Lett 585:606–612
5. Furuse M, Hata M, Furuse K, Yoshida Y, Haratake A, Sugitani Y, Noda T, Kubo A, Tsukita S (2002) Claudin-based tight junctions are crucial for the mammalian epidermal barrier: a lesson from claudin-1-deficient mice. J Cell Biol 156:1099–1111
6. Milatz S, Krug SM, Rosenthal R, Günzel D, Müller D, Schulzke JD, Amasheh S, Fromm M (2010) Claudin-3 acts as a sealing component of the tight junction for ions of either charge and uncharged solutes. Biochim Biophys Acta Biomembr 1798:2048–2057
7. Amasheh S, Schmidt T, Mahn M, Florian P, Mankertz J, Tavalali S, Gitter AH, Schulzke JD, Fromm M (2005) Contribution of claudin-5 to barrier properties in tight junctions of epithelial cells. Cell Tissue Res 321:89–96
8. Furuse M, Furuse K, Sasaki H, Tsukita S (2001) Conversion of zonulae occludentes from tight to leaky strand type by introducing claudin-2 into Madin-Darby canine kidney I cells. J Cell Biol 153:236–272
9. Amasheh S, Meiri N, Gitter AH, Schöneberg T, Mankertz J, Schulzke JD, Fromm M (2002) Claudin-2 expression induces cation-selective channels in tight junctions of epithelial cells. J Cell Sci 115:4969–4976
10. Tamura A, Hayashi H, Imasato M, Yamazaki Y, Hagiwara A, Wada M, Noda T, Watanabe M, Suzuki Y, Tsukita S (2010) Loss of claudin-15, but not claudin-2, causes Na^+ deficiency and glucose malabsorption in mouse small intestine. Gastroenterology 140:913–923
11. Günzel D, Stuiver M, Kausalya PJ, Haisch L, Rosenthal R, Krug SM, Meij IC, Hunziker W, Fromm M, Müller D (2009) Claudin-10 exists in six alternatively spliced isoforms which exhibit distinct localization and function. J Cell Sci 122:1507–1517
12. Van Itallie CM, Rogan S, Yu A, Vidal LS, Holmes J, Anderson JM (2006) Two splice variants of claudin-10 in the kidney create paracellular pores with different ion selectivities. Am J Physiol Renal Physiol 291:F1288–F1299
13. Hou J, Renigunta A, Yang J, Waldegger S (2010) Claudin-4 forms paracellular chloride channel in the kidney and requires claudin-8 for tight junction localization. Proc Natl Acad Sci USA 107:18010–18015
14. Coyne CB, Gambling TM, Boucher RC, Carson JL, Johnson LG (2003) Role of claudin interactions in airway tight junctional permeability. Am J Physiol Lung Cell Mol Physiol 285:1166–1178
15. Michikawa H, Fujita-Yoshigaki J, Sugiya H (2008) Enhancement of barrier function by overexpression of claudin-4 in tight junctions of submandibular gland cells. Cell Tissue Res 334:255–264
16. Katoh M, Katoh M (2003) CLDN23 gene, frequently downregulated in intestinal-type gastric cancer, is a novel member of CLAUDIN gene family. Int J Mol Med 11:683–689
17. Hewitt KJ, Agarwal R, Morin PJ (2006) The claudin gene family: expression in normal and neoplastic tissues. BMC Cancer 6:186
18. Gekle M, Wünsch S, Oberleithner H, Silbernagl S (1994) Characterization of two MDCK-cell subtypes as a model system to study principal cell and intercalated cell properties. Pflügers Arch 428:157–162

19. Krug SM, Amasheh S, Richter JF, Milatz S, Günzel D, Westphal JK, Huber O, Schulzke JD, Fromm M (2009) Tricellulin forms a barrier to macromolecules in tricellular tight junctions without affecting ion permeability. Mol Biol Cell 20:3713–3724
20. Kreusel KM, Fromm M, Schulzke JD, Hegel U (1991) Cl^- secretion in epithelial monolayers of mucus-forming human colon cells (HT-29/B6). Am J Physiol 261:C574–C582
21. Krug SM, Fromm M, Günzel D (2009) Two-path impedance spectroscopy for measuring paracellular and transcellular epithelial resistance. Biophys J 97:2202–2211
22. Rosenthal R, Milatz S, Krug SM, Oelrich B, Schulzke JD, Amasheh S, Günzel D, Fromm M (2010) Claudin-2, a component of the tight junction, forms a paracellular water channel. J Cell Sci 123:1913–1921
23. Zeissig S, Bürgel N, Günzel D, Richter JF, Mankertz J, Wahnschaffe U, Kroesen AJ, Zeitz M, Fromm M, Schulzke JD (2007) Changes in expression and distribution of claudin-2, -5 and -8 lead to discontinuous tight junctions and barrier dysfunction in active Crohn's disease. Gut 56:61–72
24. Stevenson BR, Anderson JM, Goodenough DA, Mooseker MS (1988) Tight junction structure and ZO-1 content are identical in two strains of Madin-Darby canine kidney cells which differ in transepithelial resistance. J Cell Biol 107:2401–2408
25. Kiuchi-Saishin Y, Gotoh S, Furuse M, Takasuga A, Tano Y, Tsukita S (2002) Differential expression patterns of claudins, tight junction membrane proteins, in mouse nephron segments. J Am Soc Nephrol 13:875–886
26. Angelow S, Kim KJ, Yu AS (2006) Claudin-8 modulates paracellular permeability to acidic and basic ions in MDCK II cells. J Physiol 571:15–26
27. Angelow S, Schneeberger EE, Yu AS (2007) Claudin-8 expression in renal epithelial cells augments the paracellular barrier by replacing endogenous claudin-2. J Membr Biol 215:147–59
28. Enck AH, Berger UV, Yu AS (2001) Claudin-2 is selectively expressed in proximal nephron in mouse kidney. Am J Physiol Renal Physiol 281:F966–F974
29. Muto S, Hata M, Taniguchi J, Tsuruoka S, Moriwaki K, Saitou M, Furuse K, Sasaki H, Fujimura A, Imai M, Kusano E, Tsukita S, Furuse M (2010) Claudin-2-deficient mice are defective in the leaky and cation-selective paracellular permeability properties of renal proximal tubules. Proc Natl Acad Sci USA 107:8011–8016
30. Furuse M, Sasaki H, Tsukita S (1999) Manner of interaction of heterogeneous claudin species within and between tight junction strands. J Cell Biol 147:891–903
31. Alpern RJ, Howlin KJ, Preisig PA (1985) Active and passive components of chloride transport in the rat proximal convoluted tubule. J Clin Invest 76:1360–1366
32. Aronson PS, Giebisch G (1997) Mechanisms of chloride transport in the proximal tubule. Am J Physiol 273:F179–F192
33. Cogan MG, Maddox DA, Lucci MS, Rector FC (1979) Control of proximal bicarbonate reabsorption in normal and acidotic rats. J Clin Invest 64:1168–1180
34. Lang F, Neuman S, Oberleithner H, Greger R, Messner G (1982) Carbonic anhydrase independent bicarbonate reabsorption. Pflügers Arch 395:121–125
35. Alpern RJ, Cogan MG, Rector FC (1982) Effect of luminal bicarbonate concentration on proximal acidification in the rat. Am J Physiol 243:F53–F59
36. Yu AS, Cheng MH, Angelow S, Günzel D, Kanzawa SA, Schneeberger EE, Fromm M, Coalson RD (2008) Molecular basis for cation selectivity in claudin-2–based paracellular pores: identification of an electrostatic interaction site. J Gen Physiol 133:111–127
37. Sansom MS, Kerr ID, Breed J, Sankararamakrishnan R (1996) Water in channel-like cavities: structure and dynamics. Biophys J 70:693–702
38. Colegio OR, Van Itallie CM, McCrea HJ, Rahner HJ, Anderson JM (2002) Claudins create charge-selective channels in the paracellular pathway between epithelial cells. Am J Physiol Cell Physiol 283:C142–C147